# *Operando* Measurement of Layer Breathing Modes in Lithiated Graphite

*Hossein Yadegari,[*,†] Mohamed A. Koronfel,[†,‡] Kang Wang,[†] Daisy B. Thornton,[†] Ifan E.L. Stephens,[†] Carla Molteni,[ə] Peter D. Haynes,[†] Mary P. Ryan[*,†]*

[†]Department of Materials, Imperial College London, London SW7 2AZ, U.K.

[‡]Diamond Light Source, Harwell Science and Innovation Campus, Didcot OX11 0DE, U.K.

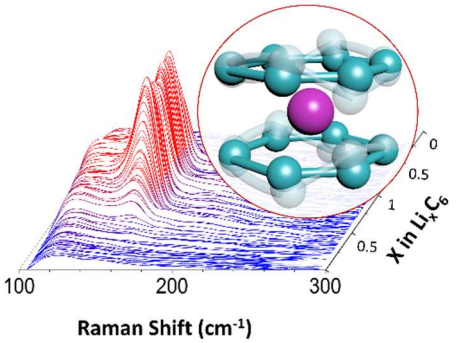
[ə]Department of Physics, King's College London, Strand, London WC2R 2LS, U.K.

**ABSTRACT**

Despite their ubiquitous usage and increasing societal dependence on Li-ion batteries, there remains a lack of detailed empirical evidence of Li intercalation/deintercalation into graphite even though this process dictates performance, longevity and safety of the system. Here, we report direct detection and dissociation of specific crystallographic phases in the lithiated graphite which form through a stepwise staging process. Using *operando* measurements, $LiC_{18}$, $LiC_{12}$ and $LiC_6$ phases are observed *via* distinct low-frequency Raman features which are the result of displacement of the graphite lattice by induced local strain. Density-functional theory calculations confirms the nature of the Raman active vibrational modes, to the layer breathing modes (LBM) of the lithiated graphite. The new findings indicate graphene-like characteristics in the lithiated graphite under the deep charged condition due to the imposed strain by the inserted Li. Moreover, our approach also provides a simple experimental tool to measure induced strain in the graphite structure under full intercalation conditions.

[*] Prof. Mary P. Ryan, E-mail: m.p.ryan@imperial.ac.uk, Dr. Hossein Yadegari, E-mail: h.yadegari@imperial.ac.uk

**TOC GRAPHICS**




Graphite has been the predominant negative electrode materials in Li-ion batteries since their commercialization in 1991.[1] The applicability of graphite in Li-ion cells was reported by Yazami for the first time when a graphite intercalated compound (GIC) was electrochemically formed using a solid organic electrolyte.[2] The obtained GIC electrode exhibited reversible Li intercalation with high chemical and thermal stability, low operation potential *vs.* $Li/Li^+$, small volume change and large specific capacity. Therefore, a GIC was used to assemble the first Li-ion cell by Yoshino despite the restricting effect of graphite on the charging rate of the cell.[1, 3] The layered structure with strong $sp^2$ C–C bonds within the planes and weak van der Waals forces between the planes makes graphite an ideal host structure for the insertion of various guest species. As a result, the electrochemical formation of GICs with alkali metal cations occurs at potentials close to the redox potentials of the corresponding metals, which is desirable for anode materials. The application of GICs as the negative electrode in sodium and potassium ion batteries has also been demonstrated.[4-6] The microstructure of the carbonaceous electrodes including the pore structure and the presence of defects is proven to be particularly important in this regard.[6]

The detailed structural changes of graphite during intercalation and deintercalation of $Li^+$ is not fully understood.[7] The most widely accepted intercalation model was introduced by Daumas-Hérold in which $Li^+$ ions can only move between the planes through a stepwise staging process.[8] Each stage is described by a stage index, *n*, representing the number of graphene layers

between two guest layers.[9] The nature of this staging process has been correlated to the repulsive forces between guest species as well as the energy required to overcome the van der Waals attraction between the graphene planes.[9] The insertion of $Li^+$ into graphite induces mechanical strain which results in structural distortion. The total volume change of $Li_xC_6$ system has been measured using *operando* X-ray diffraction (XRD) to be 6.1% for stage 2 ($x$=0.5) and 13.2% for stage 1 ($x$=0.95).[10]

Using a low energy electromagnetic probe to stimulate vibrational modes, Raman spectroscopy (RS) provides unique structural information at microscales.[11] In addition, RS is particularly attractive for *operando* studies in electrochemical systems due to the non-destructive probe, fast response time, sub-micrometer lateral resolution and simple cell design.[12] *Operando* RS (ORS) has been applied in a number of studies to investigate the intercalation of $Li^+$ into graphite. Inaba *et al.* proved that the electrochemical potential of a highly oriented pyrolytic graphite (HOPG) electrode is correlated with the intercalation stage at the electrode surface observed by ORS.[13] Thereafter, application of ORS to study Li intercalation into various GIC electrodes and using different electrolyte systems was reported.[14-18] However, all the reports so far have been focused on the changes in the characteristic features of graphite (*i.e.* the D, G and G'/2D bands) as pristine graphite does not exhibit a distinct feature in the low-frequency region. In this study, we present newly observed features at low wavenumbers for alkali metal GICs. These new results provide direct information regarding the phase changes during intercalation and deintercalation processes in graphite. The new features can be employed to further analyze the degradation process of carbonaceous electrode materials in metal-ion cells by measuring the imposed mechanical strain at different states of charge.[19] In addition, the developed approach in this study can be further expanded to other alkali metal-ion batteries such as Na- and K-ion as well as multivalent ions cells like Al-ion.

The experimental details of ORS are presented in the Supporting Information (Figures S1-2). Raman measurements were collected from a single particle during electrochemical charge/discharge. A typical galvanostatic charge/discharge profile of the half-cell cycled between 1.0 and 0.01 V vs. $Li/Li^+$ at C/20 rate is shown in Figure S3, exhibiting an average specific capacity of ~350 mAh $g^{-1}$. The multiple plateaus display different lithiation stages from

pure graphite to $LiC_6$ (see Figure S4 for staging diagram).[20] Each stage is named by a number which specifies the number of graphene layers between two intercalated layers. The letter L (liquid) refers to disordered lithium ordering. Raman spectra were recorded during electrochemical discharge/charge cycles of the cell at constant intervals. A typical Raman spectrum recorded using a fresh graphite electrode is depicted in Figure S5. The graphite electrode used in this study exhibits two main features around 1585 and 2670 $cm^{-1}$ related to the G and 2D bands, respectively. The nature of Raman peaks in carbonaceous materials has been extensively discussed before.[11, 21, 22] The G band is the main active mode in graphite, related to in-plane vibrations of $sp^2$ carbon atoms in rings and chains. In addition, a weak feature can be observed around 1350 $cm^{-1}$ (D band) which is correlated to disordered carbon structures such as presence of defects and discontinuities in crystallites.[11] The 2D band is the D band overtone but independent of defects as it originates by a process involving two phonons with opposite wave vectors.[22]

The low intensity of the D band compared to the G band ($I_D/I_G$) indicates the high crystallinity of the graphite electrode which is desirable for achieving high Li intercalation capacity.[23] Figure S6 displays chemical mapping of the D and G bands on a single particle. The chemical maps demonstrate that the electrode is mainly composed of crystalline graphite with traces of disordered carbon. Subsequently, *operando* measurements were conducted on a single spot throughout the charge/discharge cycle. The laser intensity was set to < 1 mW and Raman spectra were collected (1 s per spectrum) in 5-minute intervals to minimize the sample heating. The *operando* Raman spectra, as well as the corresponding contour plot obtained from a typical charge/discharge cycle of graphite electrode in a half-cell *vs.* Li electrode performed under C/2 rate, are shown in Figure 1. During the lithiation process, the G band initially shifts to higher wavenumbers (blue shift) and then splits into two peaks before fading into noise at the fully lithiated stage. Meanwhile, the 2D band continuously shifts toward lower wavenumbers (red shift) and similarly disappears when the GIC proceeds to stage 1. No other significant feature was detected in the range of 300 to 2900 $cm^{-1}$ (see Figure S7 for an extended range). Formation of $LiC_6$ upon insertion of Li is also associated with a color change in graphite from gray to gold (Figure S8).[24] To confirm that the electrode materials were stable under the Raman laser, five

consecutive charge/discharge cycles were recorded under operando measurement conditions (Figure S9). The reversible electrochemical cycling, along with the monotonous transformation of the Raman features, confirm the stability under the operando measurements.

The changes in the G and 2D bands of graphite during Li (de)intercalation have previously been discussed in detail.[13-15, 18, 25] The initial frequency shift in the G band mainly occurs in stage 1L–4L (see Figure S3) and has been attributed to the increase of the force constants of the in-plane C–C bonds upon Li insertion.[18] As the Li insertion proceeds, the G band broadens and splits into two distinct peaks (stages 4L–2L). The upper-frequency peak ($E_{2g2}^{(b)}$; 1605 $cm^{-1}$) is related to the boundary layers of Li-GIC and the lower-frequency peak ($E_{2g2}^{(i)}$; 1575 $cm^{-1}$) has been assigned to the interior graphene layers.[14] The intensity of the $E_{2g2}^{(b)}$ peak increases while the intensity of the $E_{2g2}^{(i)}$ peak decreases during stage 2L–2. During stage 2–1 and the formation of the highly conductive $LiC_6$ phase, the scattering intensity decreases due to the reduction in optical skin depth, resulting in the disappearance of the G band.[13] Similar steps in reverse order can be distinguished during the deintercalation process. Moreover, the shift in the 2D band has been correlated to the increase in biaxial strain on the graphene sheets induced by insertion of Li into the graphite structure. It has been demonstrated using bilayer graphene bubbles that the 2D band in graphene shifts toward lower frequencies (red shift) under biaxial strain.[26] In a similar way, the biaxial strain induced by the intercalation of Li into a graphene electrode was calculated based on the shift of the 2D band to be 0.4%.[19] The same approach obtained the biaxial strain of 0.6% for Li intercalation into the graphite electrode upon stage 2.

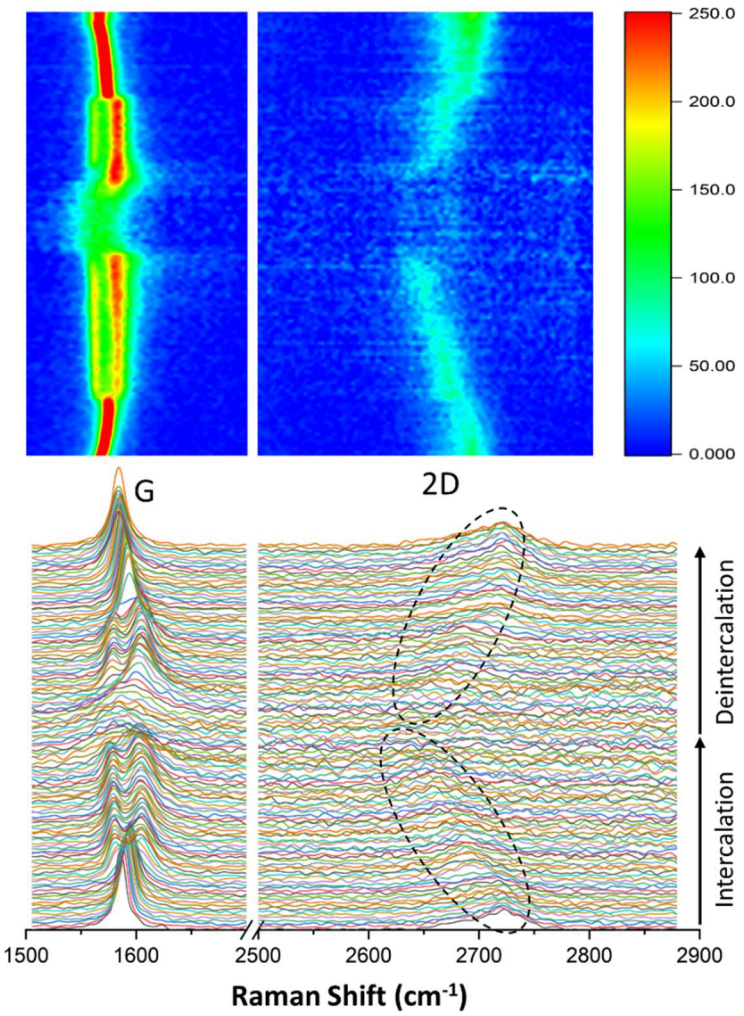



**Figure 1:** *Operando* Raman spectra and the corresponding contour plot obtained from a typical charge/discharge cycle of graphite electrode in a half-cell vs. Li electrode using a carbonate-based electrolyte performed under C/2.

Besides the well-studied in-plane vibrational modes, graphite exhibits another set of interlayer vibrational modes appearing in the low-frequency region of a Raman spectrum. These low-frequency features which originate from the relative motion of the graphene planes include shear (C) modes and layer breathing modes (LBM).[22, 27] The C mode ($E_{2g}$ at 42 $cm^{-1}$) involves the relative in-plane displacement of graphene layers and is sensitive to the interlayer coupling. Whereas LBMs are caused by out-of-plane displacements along the *c* axis, making them more sensitive to interaction *between* the graphene layers, and this is further enhanced in GICs.[27] The

latter is of particular significance in the characterization of few-layer graphene (FLG) as an interesting material for application in electronic and photonic devices.[28] Saha and colleagues investigated the vibrational properties of FLG in Bernal sequence (*AB*-stacked) using first-principles density-functional theory (DFT) calculations.[29] Their results showed that the out-of-plane transverse optical phonons ($B_{2g}$ at ~112 $cm^{-1}$) are Raman active in FLG with an even number of layers while they are optically silent in bulk graphite ($B_{1g}$ at 128 $cm^{-1}$). Moreover, the frequency of LBM is sensitive toward the number of graphene layers, stacking order and interlayer separation.[30, 31]

Nevertheless, experimental observation of these low-frequency modes is challenging due to the strong Rayleigh scattering background.[22, 29, 32] Shang *et al.* observed a single LBM at ~120 $cm^{-1}$ for FLG grown by chemical vapor deposition.[33] Subsequently, different LBM frequencies of the two-phonon overtone were reported for FLG using doubly resonant Raman spectroscopy.[27] However, previous ORS studies on GICs have been solely focused on the changes occurring to the in-plane vibrational modes (G and 2D bands).[11] By collecting a wide range of wavenumbers in an *operando* fashion, we observed a new feature in the Raman spectra of GIC during stage 2–1 (Figures 2 and S10). Figure 2 displays the *operando* Raman spectra including the low-frequency range of spectrum obtained during a charge/discharge cycle of a graphite electrode in a half-cell vs. Li electrode under C/20 rate. As the intensity of the G band decreases during stage 2–1, several low-frequency features emerge in the range of 100 to 300 $cm^{-1}$ (see also Figure S11). Similar features were observed for the charge/discharge of graphite electrode under C/10 and C/2 rates (Figures S12 and S13).

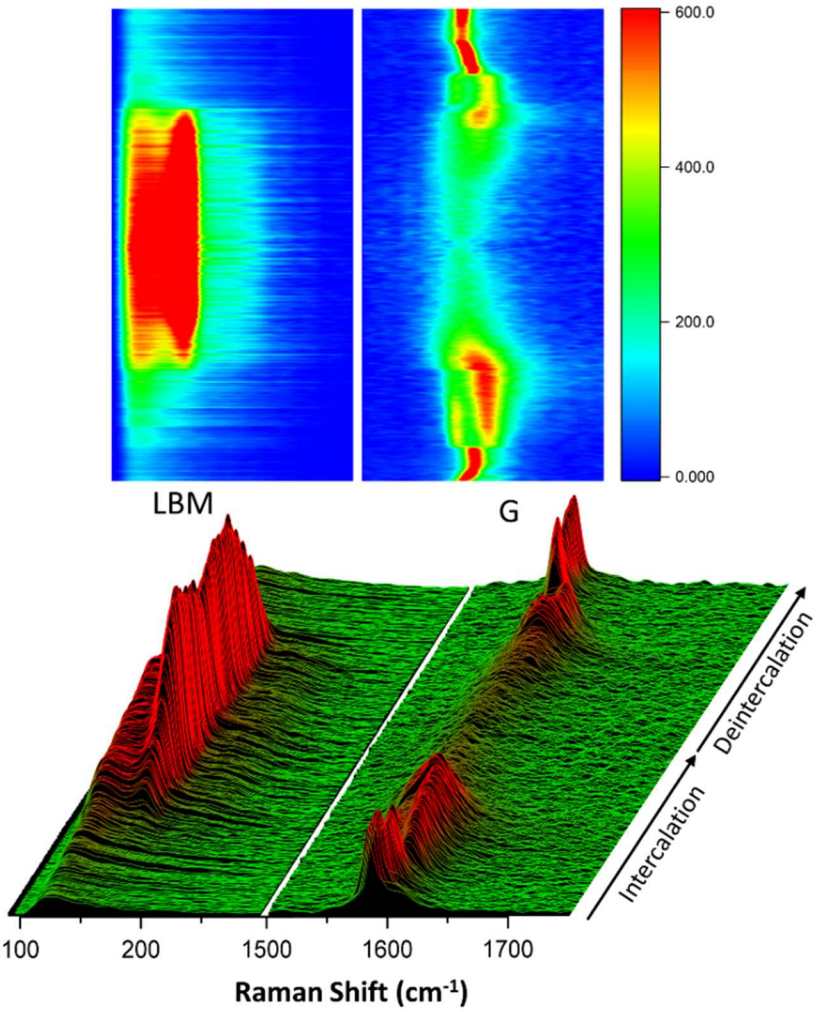



**Figure 2:** *Operando* Raman spectra and the corresponding contour plot including the low-frequency range of spectrum obtained from a charge/discharge cycle of graphite electrode in a half-cell vs. Li electrode using a carbonate-based electrolyte performed under C/20.

The low-frequency features appeared for GIC during stage 2–1 are most likely related to the out-of-plane displacement ($A_{1g}$ mode) of graphene layers adjacent to Li. It should also be noted that in contrast with FLG samples, the low-frequency features in graphite exhibit significant intensity which is comparable with the G band of pristine graphite. The higher intensity of the observed low-frequency features could be related to greater interlayer separation due to the intercalated Li which in turn reduces the van der Waals interactions between the graphene layers. To confirm the origin of these features, we derived the phonon dispersion plots for $LiC_{18}$

stacked in *AAB* sequence as well as $LiC_{12}$ and $LiC_6$ stacked in *AA* sequence using DFT calculations (see Supporting Information for calculation details).[34] Phonon dispersions were obtained using the finite difference / supercell method for $LiC_{18}$, $LiC_{12}$ and $Li_2C_{12}$ and are shown in Figure 3, where the relevant mode is highlighted in red (full-range plots are depicted in Figures S14-S16). The corresponding out-of-plane displacement patterns are also depicted in Figure 3. It should be noted that DFT calculations for $LiC_{18}$ stacked in *AA* sequence resulted in imaginary frequencies at the Γ-point, indicating the mechanical instability of the system (Figure S17). Therefore, the phonon dispersion of $LiC_{18}$ system was calculated in *AAB* sequence which is shown to be stable.[35]

Our DFT calculations reveal that Li-intercalated graphite exhibits Raman active modes in the low-frequency region. The LBM frequencies at the Γ-point were predicted by DFT to be 173, 196 and 213 $cm^{-1}$ for $LiC_{18}$, $LiC_{12}$ and $LiC_6$, respectively, which are slightly larger than, but show a similar trend to, the features observed in experiments at ~136, 162 and 205 $cm^{-1}$ (Figure S18). Meanwhile, DFT calculations did not indicate any Raman active mode in the low-frequency region for pristine graphite stacked in either *AA* or *AB* sequences (Figure S19 and S20). In addition, the low-frequency features did not appear in experiment before reaching stage 2 which is likely due to the low intensity of these features in the early, dilute, intercalated stages. The most significant change in the intensity upon Li (de)intercalation occurs for the middle-frequency feature at 162 $cm^{-1}$, whilst the least change was observed for the upper-frequency feature.

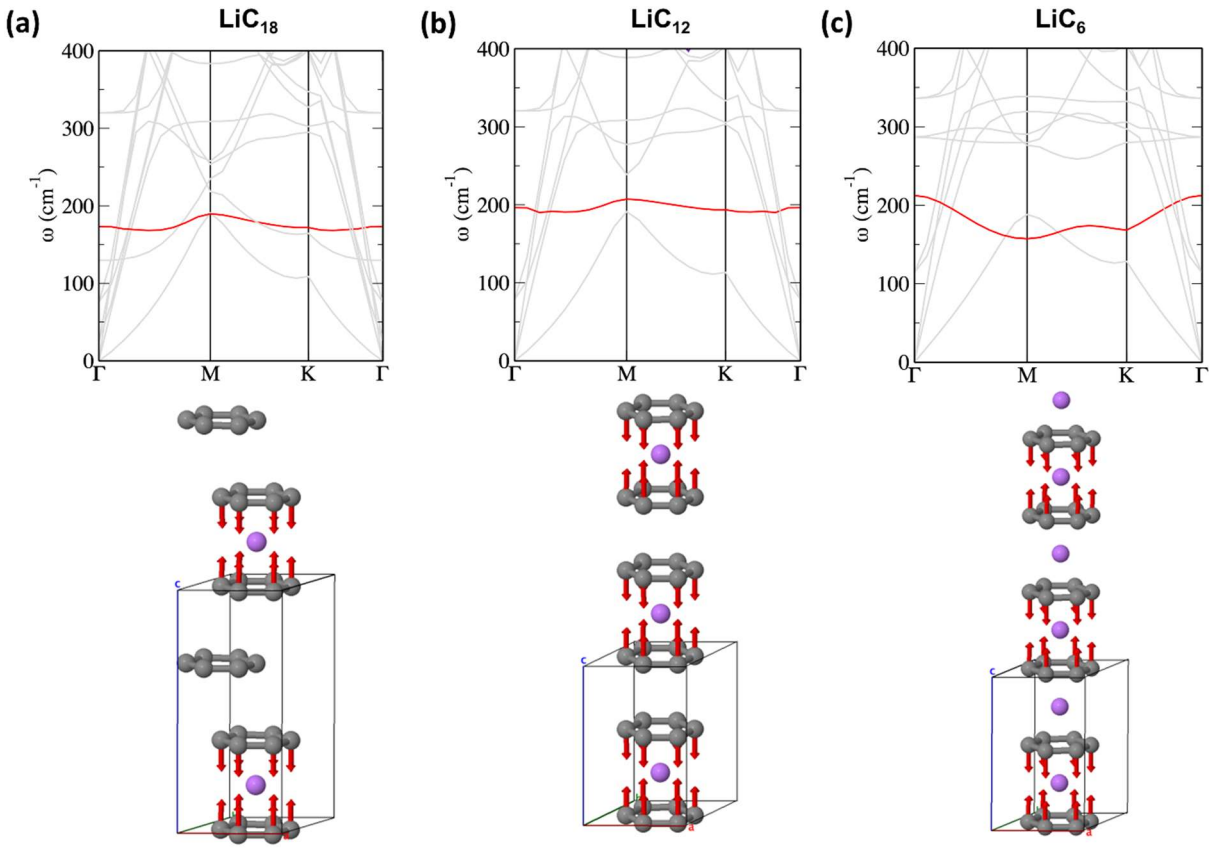



**Figure 3:** Phonon dispersion plots calculated using DFT for (a) $LiC_{18}$ system stacked in *AAB* sequence; (b) $LiC_{12}$ and (c) $LiC_6$ systems stacked in *AA* sequence. The low-frequency Raman active mode is shown in red. The corresponding displacement patterns for the indicated Raman active mode are also depicted.

The experimental spectra at different points during stage 2–1 of Li intercalation and deintercalation were fitted with three Lorentzian peaks as shown in Figure S21. The areas under the deconvoluted peaks are plotted against discharge/charge time in Figure 4a. The evolution of the peaks during the intercalation and deintercalation processes is not symmetric, which is due to slight differences between the two phenomena.[13, 18] Based on the changes in the corresponding peak areas and assigning the observed features to different GIC phases according to the DFT results, it appears that the $LiC_{18}$ and $LiC_{12}$ phases increase during the first 5 hours of stage 2–1, then stay unchanged until 2.5 h into the deintercalation before starting to decrease. The formation of the $LiC_6$ phase, however, only begins when $LiC_{18}$ and $LiC_{12}$ saturate. The $LiC_6$ phase shows a decrease at the end of intercalation and beginning of deintercalation

before exhibiting a second increase. The more variable changes in the $LiC_6$ phase could be related to disproportionation to other phases. These results suggest that different phases *coexist* during stage 2–1 of Li intercalation into graphite, as schematically shown in Figure 4b.

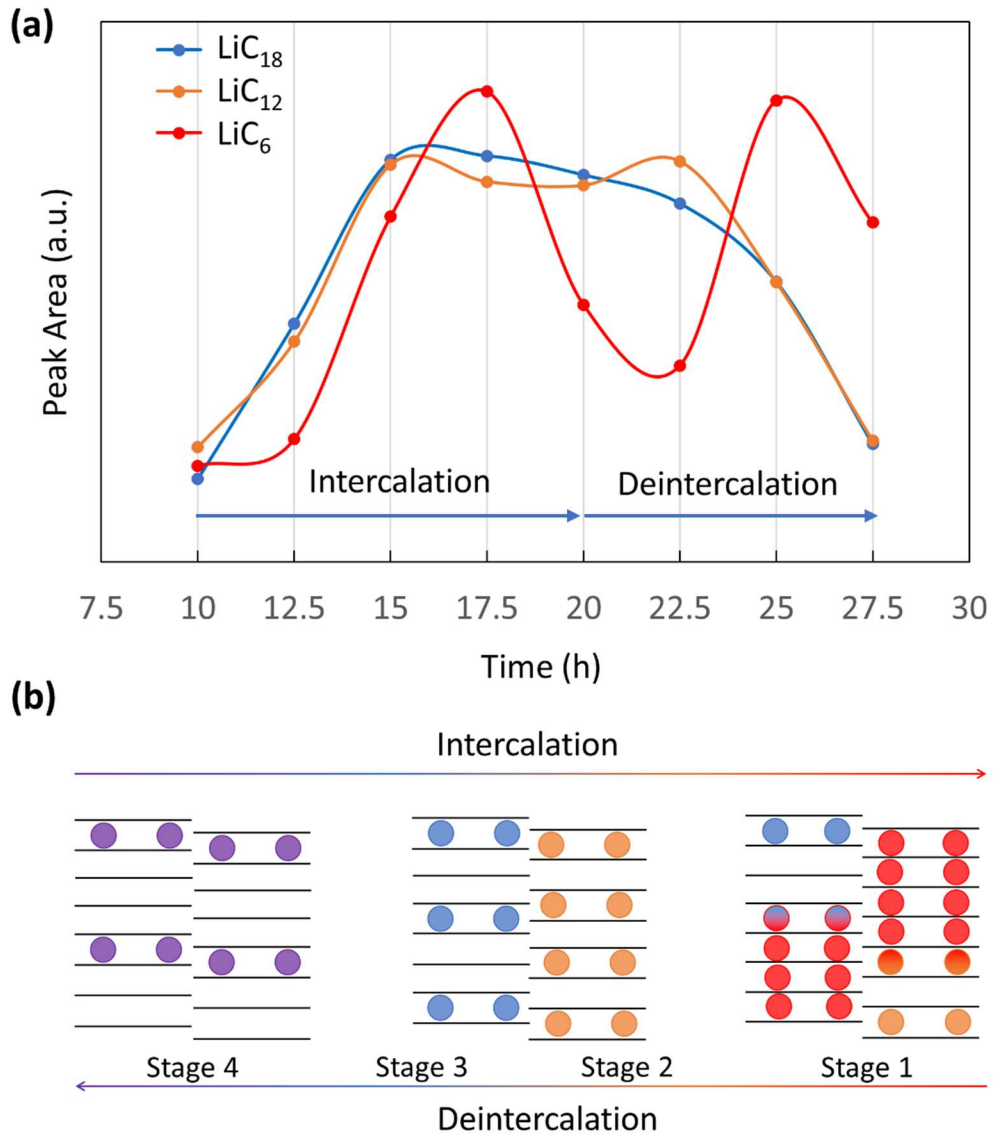



**Figure 4:** (a) the relative area of the deconvoluted Raman peaks for $LiC_{18}$, $LiC_{12}$ and $LiC_6$ phases obtained from the data shown in Figure 2 plotted against discharge/charge time; (b) schematic diagram of the intercalation/deintercalation processes. Different colors represent Li ions in various $LiC_X$ phases.

The data obtained in this study demonstrate, for the first time, the low-frequency LBM features in the Raman spectra of Li-GIC during stage 2–1 of (de)intercalation process under *operando* condition. DFT calculations revealed that different intercalated phases exhibit distinct Raman active features at the low-frequency region originating from out-of-plane displacement of graphene layers adjacent to Li. The appearance of these LBM features during stage 2–1 of Li intercalation/deintercalation indicates that graphite displays FLG characteristics in terms of its electronic and geometrical structures when deeply intercalated. In addition, the co-existence of multiple phases was concluded during stage 2–1 based on assigning the observed experimental features according to the DFT calculations. Furthermore, the low-frequency LBM features provide a simple experimental tool to measure the induced strain in the graphite structure under deep intercalation conditions where the G and 2D peaks are absent. Comparison of low-frequency Raman response of GIC with other guest species such as $Na^+$ and $K^+$ will be of particular interest in this regard. More detailed studies are required to thoroughly unveil the phase changes occurring during the intercalation and deintercalation processes in GIC.

## ASSOCIATED CONTENT

### Supporting Information

The Supporting Information is available free of charge on the ACS Publications website at DOI: XXXX. Experimental details, electrochemical and spectroscopic data, calculation results.

## AUTHOR INFORMATION

### Corresponding Authors

Hossein Yadegari - Department of Materials, Imperial College London, London SW7 2AZ, U.K.; Email: h.yadegari@imperial.ac.uk

Mary P. Ryan - Department of Materials, Imperial College London, London SW7 2AZ, U.K.; Email: m.p.ryan@imperial.ac.uk

Authors

Mohamed A. Koronfel - Department of Materials, Imperial College London, London SW7 2AZ, U.K.; Diamond Light Source, Harwell Science and Innovation Campus, Didcot OX11 0DE, U.K.

Kang Wang - Department of Materials, Imperial College London, London SW7 2AZ, U.K.

Daisy B. Thornton - Department of Materials, Imperial College London, London SW7 2AZ, U.K.

Ifan E.L. Stephens - Department of Materials, Imperial College London, London SW7 2AZ, U.K.

Carla Molteni - Department of Physics, King's College London, Strand, London WC2R 2LS, U.K.

Peter D. Haynes - Department of Materials, Imperial College London, London SW7 2AZ, U.K.

ACKNOWLEDGMENT

This work was supported by the ISCF Faraday Challenge project: ''Towards a Comprehensive Understanding of Degradation Processes in EV Batteries'' and the financial support is gratefully acknowledged. MPR gratefully acknowledges support from the Royal Academy of Engineering. Support from the Thomas Young Centre is acknowledged under grant number TYC-101. Calculations were performed on the Imperial College London Research Computing Service.

## REFERENCES


1. Goodenough, J. B.; Park, K. S., The Li-Ion Rechargeable Battery: A Perspective. *J. Am. Chem. Soc.* **2013,** *135* (4), 1167-1176.

2. Yazami, R.; Touzain, P., A Reversible Graphite Lithium Negative Electrode for Electrochemical Generators. *J. Power Sources* **1983,** *9* (3-4), 365-371.

3. Yoshino, A.; Sanechika, K.; Nakajima, T. Secondary Battery. U.S. Patent 4,668,595, May 26, 1987.

4. Jache, B.; Adelhelm, P., Use of graphite as a highly reversible electrode with superior cycle life for sodium-ion batteries by making use of co-intercalation phenomena. *Angew. Chem. Int. Ed. Engl.* **2014,** *53* (38), 10169-10173.

5. Jian, Z. L.; Luo, W.; Ji, X. L., Carbon Electrodes for K-Ion Batteries. *J. Am. Chem. Soc.* **2015,** *137* (36), 11566-11569.

6. Li, Y. Q.; Lu, Y. X.; Meng, Q. S.; Jensen, A. C. S.; Zhang, Q. Q.; Zhang, Q. H.; Tong, Y. X.; Qi, Y. R.; Gu, L.; Titirici, M. M.; Hu, Y. S., Regulating Pore Structure of Hierarchical Porous Waste Cork-Derived Hard Carbon Anode for Enhanced Na Storage Performance. *Adv. Energy Mater.* **2019,** *9* (48) 1902852.

7. Li, Y.; Lu, Y. X.; Adelhelm, P.; Titirici, M. M.; Hu, Y. S., Intercalation chemistry of graphite: alkali metal ions and beyond. *Chem. Soc. Rev.* **2019,** *48* (17), 4655-4687.

8. Allart, D.; Montaru, M.; Gualous, H., Model of Lithium Intercalation into Graphite by Potentiometric Analysis with Equilibrium and Entropy Change Curves of Graphite Electrode. *J. Electrochem. Soc.* **2018,** *165* (2), A380-A387.

9. Winter, M.; Besenhard, J. O.; Spahr, M. E.; Novak, P., Insertion electrode materials for rechargeable lithium batteries. *Adv. Mater.* **1998,** *10* (10), 725-763.

10. Schweidler, S.; de Biasi, L.; Schiele, A.; Hartmann, P.; Brezesinski, T.; Janek, J., Volume Changes of Graphite Anodes Revisited: A Combined Operando X-ray Diffraction and In Situ Pressure Analysis Study. *J. Phys. Chem. C* **2018,** *122* (16), 8829-8835.

11. Baddour-Hadjean, R.; Pereira-Ramos, J. P., Raman microspectrometry applied to the study of electrode materials for lithium batteries. *Chem. Rev.* **2010,** *110* (3), 1278-319.

12. Yadegari, H.; Banis, M. N.; Lin, X. T.; Koo, A.; Li, R. Y.; Sun, X. L., Revealing the Chemical Mechanism of $NaO_2$ Decomposition by In Situ Raman Imaging. *Chem. Mater.* **2018,** *30* (15), 5156-5160.

13. Inaba, M.; Yoshida, H.; Ogumi, Z.; Abe, T.; Mizutani, Y.; Asano, M., In-Situ Raman-Study on Electrochemical Li-Intercalation into Graphite. *J. Electrochem. Soc.* **1995,** *142* (1), 20-26.

14. Panitz, J. C.; Joho, F.; Novak, P., In situ characterization of a graphite electrode in a secondary lithium-ion battery using Raman microscopy. *Appl. Spectrosc.* **1999,** *53* (10), 1188-1199.

15. Hardwick, L. J.; Buqa, H.; Holzapfel, M.; Scheifele, W.; Krumeich, F.; Novak, P., Behaviour of highly crystalline graphitic materials in lithium-ion cells with propylene carbonate containing electrolytes: An in situ Raman and SEM study. *Electrochim. Acta* **2007,** *52* (15), 4884-4891.

16. Hardwick, L. J.; Ruch, P. W.; Hahn, M.; Scheifele, W.; Kotz, R.; Novak, P., In situ Raman spectroscopy of insertion electrodes for lithium-ion batteries and supercapacitors: First cycle effects. *J. Phys. Chem. Solids* **2008,** *69* (5-6), 1232-1237.

17. Sethuraman, V. A.; Hardwick, L. J.; Srinivasan, V.; Kostecki, R., Surface structural disordering in graphite upon lithium intercalation/deintercalation. *J. Power Sources* **2010,** *195* (11), 3655-3660.

18. Sole, C.; Drewett, N. E.; Hardwick, L. J., In situ Raman study of lithium-ion intercalation into microcrystalline graphite. *Faraday Discuss.* **2014,** *172*, 223-37.

19. Song, H. B.; Xie, H. M.; Xu, C. C.; Kang, Y. L.; Li, C. W.; Zhang, Q., In Situ Measurement of Strain Evolution in the Graphene Electrode during Electrochemical Lithiation and Delithiation. *J. Phys. Chem. C* **2019,** *123* (31), 18861-18869.

20. Hess, M.; Novak, P., Shrinking annuli mechanism and stage-dependent rate capability of thin-layer graphite electrodes for lithium-ion batteries. *Electrochim. Acta* **2013,** *106*, 149-158.

21. Ferrari, A. C., Raman spectroscopy of graphene and graphite: Disorder, electron-phonon coupling, doping and nonadiabatic effects. *Solid State Commun.* **2007,** *143* (1-2), 47-57.

22. Ferrari, A. C.; Basko, D. M., Raman spectroscopy as a versatile tool for studying the properties of graphene. *Nat Nanotechnol* **2013,** *8* (4), 235-246.

23. Ji, K.; Han, J.; Hirata, A.; Fujita, T.; Shen, Y.; Ning, S.; Liu, P.; Kashani, H.; Tian, Y.; Ito, Y.; Fujita, J. I.; Oyama, Y., Lithium intercalation into bilayer graphene. *Nature communications* **2019,** *10* (1), 275.

24. Harris, S. J.; Timmons, A.; Baker, D. R.; Monroe, C., Direct in situ measurements of Li transport in Li-ion battery negative electrodes. *Chem. Phys. Lett.* **2010,** *485* (4-6), 265-274.

25. Hardwick, L. J.; Ruch, P. W.; Hahn, M.; Scheifele, W.; Kötz, R.; Novák, P., In situ Raman spectroscopy of insertion electrodes for lithium-ion batteries and supercapacitors: First cycle effects. *J. Phys. Chem. Solids* **2008,** *69* (5-6), 1232-1237.

26. Zabel, J.; Nair, R. R.; Ott, A.; Georgiou, T.; Geim, A. K.; Novoselov, K. S.; Casiraghi, C., Raman Spectroscopy of Graphene and Bilayer under Biaxial Strain: Bubbles and Balloons. *Nano Lett.* **2012,** *12* (2), 617-621.

27. Lui, C. H.; Heinz, T. F., Measurement of layer breathing mode vibrations in few-layer graphene. *Physical Review B* **2013,** *87* (12), 121404(R).

28. Tan, P. H.; Han, W. P.; Zhao, W. J.; Wu, Z. H.; Chang, K.; Wang, H.; Wang, Y. F.; Bonini, N.; Marzari, N.; Pugno, N.; Savini, G.; Lombardo, A.; Ferrari, A. C., The shear mode of multilayer graphene. *Nat Mater* **2012,** *11* (4), 294-300.

29. Saha, S. K.; Waghmare, U. V.; Krishnamurthy, H. R.; Sood, A. K., Phonons in few-layer graphene and interplanar interaction: A first-principles study. *Physical Review B* **2008,** *78* (16), 165421.

30. Lui, C. H.; Malard, L. M.; Kim, S.; Lantz, G.; Laverge, F. E.; Saito, R.; Heinz, T. F., Observation of layer-breathing mode vibrations in few-layer graphene through combination Raman scattering. *Nano Lett.* **2012,** *12* (11), 5539-5544.

31. Liang, L.; Zhang, J.; Sumpter, B. G.; Tan, Q. H.; Tan, P. H.; Meunier, V., Low-Frequency Shear and Layer-Breathing Modes in Raman Scattering of Two-Dimensional Materials. *Acs Nano* **2017,** *11* (12), 11777-11802.

32. Lin, M.-L.; Wu, J.-B.; Liu, X.-L.; Tan, P.-H., Probing the shear and layer breathing modes in multilayer graphene by Raman spectroscopy. *Journal of Raman Spectroscopy* **2018,** *49* (1), 19-30.

33. Shang, J.; Cong, C.; Zhang, J.; Xiong, Q.; Gurzadyan, G. G.; Yu, T., Observation of low-wavenumber out-of-plane optical phonon in few-layer graphene. *Journal of Raman Spectroscopy* **2013,** *44* (1), 70-74.

34. Clark, S. J.; Segall, M. D.; Pickard, C. J.; Hasnip, P. J.; Probert, M. J.; Refson, K.; Payne, M. C., First principles methods using CASTEP. *Zeitschrift Fur Kristallographie* **2005,** *220* (5-6), 567-570.

35. Hazrati, E.; de Wijs, G. A.; Brocks, G., Li intercalation in graphite: A van der Waals density-functional study. *Physical Review B* **2014,** *90* (15), 155448.